THE JOURNAL OF
PHYSICAL CHEMISTRY C

ARTICLE

pubs.acs.org/JPCC

Scatter-Free IR Absorption Spectra of Individual, 3−5 μm, Airborne Dust Particles Using Plasmonic Metal Microarrays: A Library of 63 Spectra

Katherine E. Cilwa, Matthew McCormack, Michelle Lew, Christophe Robitaille, Lloyd Corwin, Marvin A. Malone, and James V. Coe*

Department of Chemistry, 100 West 18th Avenue, The Ohio State University, Columbus, Ohio 43210-1173, United States

Supporting Information

ABSTRACT: While the concentration of airborne particulate matter is well-known to be correlated with people's health, a chemical evaluation must also be important. Noting that airborne dust particles in the 3−5 μm size regime are among the largest that get into people's lungs, such particles were collected by pumping air through plasmonic metal films with a 12.6 μm square lattice of 5 μm square holes. Capture of a dust particle in a metallic hole enables the recording of "scatter-free" infrared absorption spectra whose peaks reveal the infrared active components. The study of the spectra of individual particles allows minority components to be characterized in a way that is quite incisive which is difficult with bulk samples. A library of 63 spectra of individual particles captured from our laboratory air is presented along with a preliminary analysis of the contributing components.

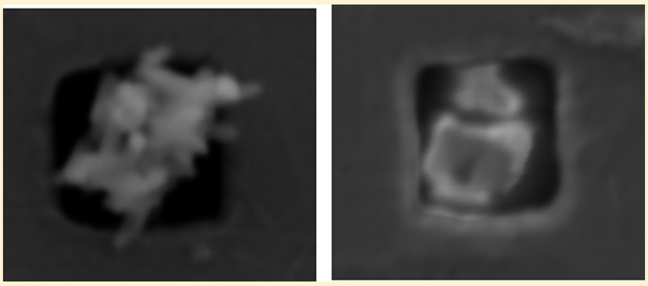

INTRODUCTION

"Indoors or outdoors, dust is unavoidable. And a marvellous fraction of that dust holds the secret to our past".[1] Dust is collected from outer space to learn about earlier times in our solar system.[2−4] Minerals from soil, volcanic eruptions, pollution, biological material, and meteorites[5] all contribute to dust in our atmosphere. Skin cells, pollen, fabric fibers, hair, road dust, local soil, agricultural fertilizers, minerals from deserts halfway around the world, and just about any other material found in the local environment contribute to the dust in our homes and workplaces. Interest in the characterization of dust, or particulate matter, spans a wide range of fields including environmental science,[6,7] atmospheric[8,9] and geological studies,[7,10−13] health-related industries,[14,15] and astronomy.[16−18] While the majority of atmospheric particulate matter is natural in origin, the remaining source of particles is anthropogenic (estimates range from 6 to 23% percent[19]) providing evidence of human environmental impact. Libraries of infrared (IR) spectra of single dust particles have the potential to address mankind's impact on the environment.

Examination of wavelength-scale particles[2] with IR microscopy provides vital, nondestructive chemical information but is limited by two major problems: (1) spectra of wavelength-sized particles are dominated by Mie scattering effects and the Christiansen effect[20,21] (vibrational line shape distortions), and (2) insignificant intensity of light is transmitted with conventional techniques through apertures as size is reduced to the range of microsized particles. Single-particle studies can be accomplished using synchrotron free electron lasers with IR microscopy adaptations. Such systems have ∼1000 times more IR power (although at significantly more expense) than the blackbody sources of benchtop Fourier transform IR (FTIR) instruments and have been used to study dust grains collected from space.[22,23] However, this method still falls prey to scattering problems that could, for instance, require mechanical crushing of some samples.[23] Our solution places the particle within a comparably sized hole of an IR plasmonic metal film with an array of such holes—to provide a metallic, but transmitting, confinement for the particle.

There have been a number of reviews,[24,25] much previous work,[26−54] and several enhanced spectroscopic techniques[25,45,46,48,55−59] on plasmonic metal films perforated with arrays of subwavelength holes, i.e., mesh. A scanning electron microscope (SEM) of our mesh is given in Figure 1a (JEOL JSM-5500 instrument). The mesh is made of Ni, has a square lattice parameter of 12.6 μm, square holes of ∼5 μm width, and a thickness of ∼2 μm, and is available from Precision Eforming. The zero-order transmission spectrum from a desktop FTIR at perpendicular incidence is contrasted with the FTIR microscope spectrum (Perkin-Elmer Spotlight 300) of the same piece of mesh in Figure 1c. The microscope focuses a ring of light with angles ranging from 17 to 37° relative to the microscope axis which both disperses plasmonic resonances and collects higher order diffraction spots. These features are good for recording

Received: June 8, 2011
Revised: July 25, 2011
Published: July 27, 2011

dx.doi.org/10.1021/jp205383h | J. Phys. Chem. C 2011, 115, 16910–16919

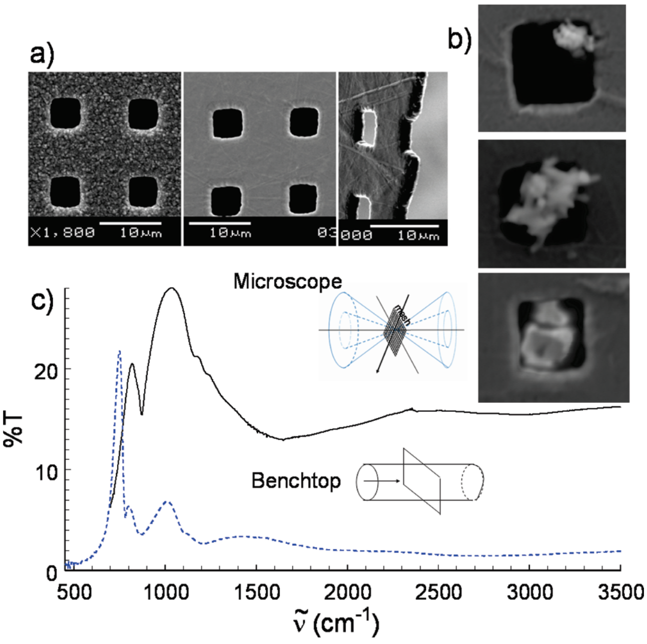

Figure 1. (a) Scanning electron microscope (SEM) images of the Ni plasmonic mesh showing, from left to right, the back side, front side, and thickness of the mesh, (b) SEM images of dust particles that have been trapped in the holes of the plasmonic metal mesh, and (c) zero-order, IR transmission spectrum of plasmonic Ni mesh in a benchtop FTIR (lower, dotted trace) and a transmission spectrum of the same piece of mesh in an FTIR microscope. The spectrum from the microscope makes a much better background for full-range IR spectral studies, while the benchtop FTIR shows more definitive plasmonic resonances. Note, however, the microscope spectrum is quite plasmonic in spite of extensive dispersion of the resonances.

spectra of particles, but bad for narrow and identifiable resonances. Greatly reduced scattering effects and undistorted absorption line shapes have been demonstrated[40] by us for individual particles by placing 5 μm diameter latex (polystyrene) spheres within the ~5 μm wide holes of this metal mesh. The method uses a benchtop FTIR microscope, i.e., an instrument which is considerably less expensive and more convenient to use than a synchrotron. Other recent work[54] involved detecting absorbance as a function of distance from an absorbing line of microspheres on mesh (as imaged with the IR microscope) showing that the plasmonic light predominately travels to the next hole before coupling back into the beam without scattering. In the course of this investigation, an inadvertent dust particle was noticed which was adversely affecting the signal averaging strategy. It became apparent that it was relatively easy to record a scatter-free, IR absorption spectrum of a single, isolated 3 μm dust particle. Dust particles can be collected on purpose by sucking air through the mesh with a small pump, and SEM images of dust particles collected in this manner are shown in Figure 1b (JEOL JSM-5500 instrument). The new IR method can be described as the wedding of metallic confinement at the scale of the particle size with a plasmonically transmitting cavity. The light incident on the metal excites surface plasmon polaritons that run along the surfaces of the mesh and couple with cavity modes of the holes resulting in transmission without scattering from the beam. It constitutes a new method for the study of individual micrometer-scale dust particles which might be useful in a variety of dust-related sciences. It should be complementary to other methods of studying single dust particles, including (to name only a few) mass spectrometry,[60−62] electron microscopy and X-ray methods,[63−66] and Raman spectroscopy.[67,68] This new method will make possible the study of a greater number and variety of particles facilitating a catalog library approach to particles within this size range.

These particles turn out to have great significance in human health. Airborne particles of about 3−5 μm diameter are among the largest globular particles that get past the filtering of the nose and throat making it into the lungs; i.e., they are respirable. A typical urban concentration of airborne particulate matter is ~30 μg/m^3. A rise of only 10 μg/m^3 from such typical values has been correlated with a rise of 0.25% in all-cause human mortality rate[69] and a rise of ~0.75% in respiratory-related mortality rate. It has also been correlated with stroke which leaves one wondering how the breathing of particulate matter could affect the cardiovascular system.[14] To make this point more dramatically, it is thought that particulate matter rose to as much as 14 000 μg/m^3 during the great London Smog Disaster[19] (p 2 therein) in 1952 in which at least 4000 people were killed as a result. In fact, the EPA regulates particulate matter with a national ambient air quality standard of an annual mean of 15 μg/m^3 and a 24 h mean of 35 μg/m^3 for particulate matter smaller than 2.5 μm (PM$_{2.5}$). The standard for particulate matter smaller than 10 μm is a 24 h average of 150 μg/m^3. Respirable dust particles in the 3−5 μm range fall between the "fine" and "course" designations and are under increased scrutiny by the EPA. Since larger particles are not likely to travel as far as smaller ones, the chemical identity of larger particles may be more reflective of local environmental challenges. There are many known diseases associated with occupations involving the specific dusts breathed by workers,[19,69−71] such as silicosis (from cutting sandstone), asbestosis or mesothelioma (from asbestos mining, milling, or fireproofing), and black lung disease (coal dust). Therefore the chemical characterization of respirable dust particles is an important matter.

■ EXPERIMENTAL SECTION

A method was devised to pump air through the metal mesh collecting dust particles in the holes. A piece of mesh (as pictured in the Figure 1a) was taped over an 1/8 in. (3.18 mm) diameter hole in a 25 mm diameter circular piece of stainless steel shimstock. The mesh/shimstock construction effectively replaces conventional 25 mm air filters and was used in a standard size, 25 mm inline Derlin Filter Holder made by SKC Inc. A Quik Start vacuum pump drew air from room 0055 of Evans Lab on the campus of the Ohio State University through the assembly at 5.0 L/min (as measured with a flow meter) for 18 h on April 21, 2010, which was a clear day, with an average temperature of 12 °C and an average relative humidity of 47%. The process of pumping air through the mesh precludes the capture of liquid aerosol particles and likely provides some drying action, so the sample consists of solid particles that were used with no further processing (such as drying). SEM images of dust particles caught in mesh holes by this method are shown in Figure 1b.

IR spectra were recorded using a Perkin-Elmer Spotlight 300 imaging FTIR microscope system with an array of 16, liquid nitrogen cooled, mercury cadmium telluride (MCT) detectors. The mesh/shimstock assembly was placed directly over a 1/2 in. diameter hole in an aluminum microscope slide which was positioned at the focus of the Cassegrain microscope system (NA = 0.6), and so the mesh was freestanding; i.e., the supporting substrate was air. Spectra were recorded in 34 different, variable

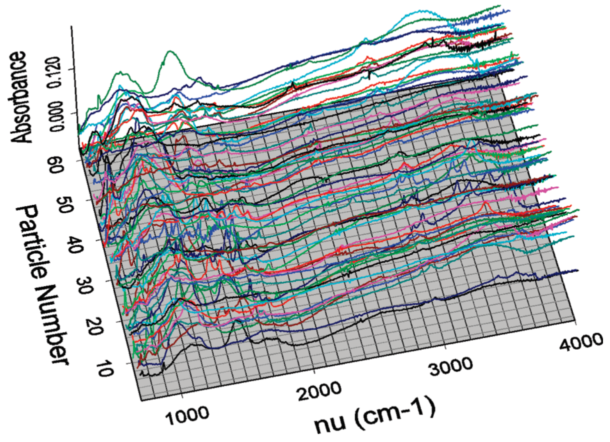

Figure 2. Scatter-free IR absorption spectra of 63 individual dust particles showing that there are extensive differences.

size regions of the mesh in imaging mode (700−4000 cm^{-1} range, 4 cm^{-1} resolution, 6.25 μm pixel size, 512 scans per pixel). The background detector curve was obtained from a 50 μm by 50 μm region of empty mesh that has a spectrum similar to the top trace in Figure 1c. This choice is best for recording spectra because it ratios away the plasmonic resonances. A typical imaging region was perhaps 100 μm by 100 μm, and an IR spectrum was recorded at every intersecting point of a 6.25 μm square grid within the region. Spectra were only acquired when the dust particle was isolated by empty surrounding holes. The 1/e propagation distance along the surface for absorption at 1424 cm^{-1} is 6.0 ± 0.3 μm.[72] This work resulted in spectra of 63 individual, isolated dust particles which required about 72 h of total scanning.

The extraction of a spectrum of an individual dust particle was performed in an identical manner for each particle preserving absolute intensity information in the spectrum. The ChemiMap function of the Perkin-Elmer SpectrumIMAGE software was used to create an absorbance contour plot at a chosen wavenumber (generally a strong vibrational feature). This plot was compared visually to the corresponding optical image to locate the particle in the IR image (there can be shifts between the IR and optical images). A 3 by 3 pixel box (18.75 μm by 18.75 μm) was drawn around the dust particle and all transmission spectra within the box were averaged (using the "coadd" function), and then the same size box was centered about a nearby empty hole and all transmission spectra within were coadded. Finally, the averaged transmission spectrum of the dust particle was ratioed to that of the empty hole, and the result was converted to absorbance units $[-\log(t_{dust}/t_{empty})]$. Calibrating experiments using Mie theory and a single 5.0 μm latex sphere show that the 3 by 3 pixel window acts like an effective window that is 19.3 μm by 19.3 μm, which allows one to convert a measured extinction spectrum to absolute cross section units.[73,74] All 63 dust particles were analyzed in this way, so their intensities are meaningful in absolute terms, as well as relative to each other. The absorption spectra of all 63 particles have been presented in Figure 2. These particles are labeled and numbered d1 through d63 where "d" stands for "dust". Note, that we have previously shown (using 5.0 μm latex microspheres and yeast cells)[40,74] that trapping a particle in the mesh hole eliminates the Mie scattering signals usually exhibited by wavelength-sized particles, as well as vibrational line shape distortions (Christensen effect).[75] The digital trace of each spectrum has been provided as a column in a text file in the Supporting Information. Peak positions were extracted from each spectrum using the Perkin-Elmer "peak find" function and were used to identify recognizable components. A file lists the peak positions in each spectrum and has also been provided with the Supporting Information. This data set can be used to quantify the occurrence of various components.

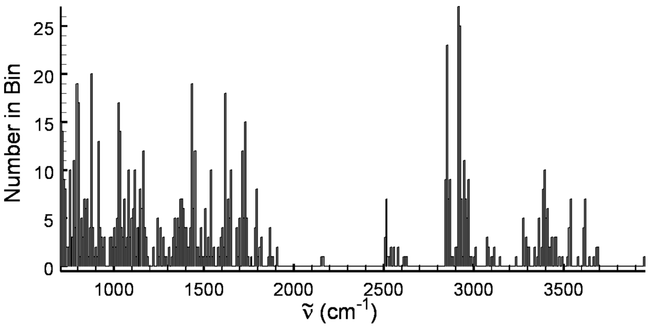

Figure 3. Histogram of the 897 peaks found in all spectra from the library of 63 individual dust particles.

RESULTS

The 63 individual dust particle spectra are generally different from each other, although they share variable amounts of common features. The majority of spectra are mixtures of two or more substances, although there are a few that appear to be mostly one material (serving as welcome indicators of correlated vibrations). Each spectrum was processed with the Perkin-Elmer "autosmooth" function, and the smoothed spectrum was searched for peaks with the "label peaks" feature with a threshold of 0.0010. This produced 897 peaks in the 63 spectra, i.e., an average of more than 14 peaks per spectrum. A histogram of the peaks was created using 8 cm^{-1} width bins as shown in Figure 3. The most common peaks appear to be the symmetric (~2855 cm^{-1}) and asymmetric (~2920 cm^{-1}) CH_2 stretches with a 1:2 intensity pattern that is characteristic of aliphatic organic matter. These peaks frequently occur as minority contributions to majority mineral components. Many of the other peaks correspond to common mineral materials like quartz (sand or chert), limestone (calcium carbonate), dolomite (calcium magnesium carbonate), gypsum ($CaSO_4 \cdot 2H_2O$), clays (kaolinite, montmorillonite, or illite), and nitrates. While some of this was expected from the IR studies of Hobert[76] using bulk dust samples, the study of individual particles offers new opportunities for analysis—particularly for characterizing minority components and the nature of the organics.

Quartz. The most common mineral appears to be quartz (crystalline SiO_2) or sand/glass (amorphous SiO_2).[77,78] Particles d3, d24, d38, d41, d42, d51, and d59 are quartz-dominated, and representative spectra are shown in Figure 4. Quartz is birefringent and exhibits both extraordinary and ordinary IR spectra.[79] The strongest band in a quartz crystal spectrum is an asymmetric SiO_4 stretch that occurs at 1080 cm^{-1} in the extraordinary beam ($E \parallel$ to the c-axis) and at 1072 cm^{-1} in the ordinary beam ($E \perp$ c-axis).[80] In powder spectra (averaged over orientations), a broader peak has been reported at 1066 cm^{-1}.[78] This band is so strong that its intensity in cross section units is bigger than the physical cross section of the particle. In general this leads to particle saturation effects, i.e., line shape broadening and breaking into multiple peaks, as predicted with Mie theory.[72] A more definitive assignment is gained through the less intense peaks at 778 cm^{-1}

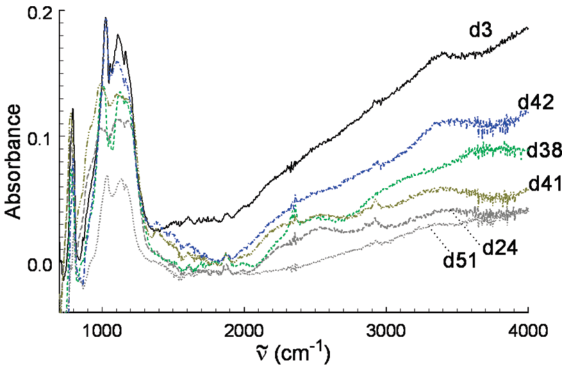

Figure 4. IR absorption spectra of six particles dominated by quartz. The main feature at ∼1000 cm^{-1} is saturating for a particle of this size (3−5 μm).

(extraordinary) and 797 cm^{-1} (ordinary). In a quartz-dominated dust particle at 4 cm^{-1} resolution, these bands appear as an almost resolved doublet whose intensities vary with the specific orientation of the particle. There is also an ordinary peak at 1163 cm^{-1}. The d3, d42, and d51 particles have orientations dominated by the ordinary spectrum, while the d24, d38, and d41 are dominated by the extraordinary spectrum. By considering all of the quartz dominated spectra as a group, bands at 1608 ± 8 and 1872 ± 7 cm^{-1}, as well as very broad bands in the 3300−3700 cm^{-1} region, are attributed to overtones and/or combination bands of quartz as can be seen in Figure 4 with quartz-dominated spectra. In addition to dust particles dominated by quartz, characteristic bands of SiO_2 were found in 54% of the individual spectra. Quartz is the most common, single, mineral component in our laboratory air.

Carbonate. Sedimentary carbonate rocks [predominantly limestone, $CaCO_3$, and dolomite, $CaMg(CO_3)_2$] readily weather and comprise about 10% of the exposed sedimentary record.[81] Like quartz, both $CaCO_3$ and $CaMg(CO_3)_2$ have birefringent crystals. Crystal spectra of carbonates have three, IR-active, CO_3^{2-} vibrations that characteristically shift by weaker interactions with different cations. Carbonate spectra are dominated by the ordinary ν_3 CO_3^{2-} antisymmetric stretch (1407 cm^{-1} in $CaCO_3$ crystal[82,83] and 1454 cm^{-1} in dolomite[83]). This peak has a $CaCO_3$ crystal vibrational intensity so strong that the cross section is bigger than the physical cross section of the particle, just like quartz, so one can expect extensive particle saturation effects such as peak broadening, line shape distortion, breaking into multiple peaks, and dispersion shifts with orientation. Other than seeing a broad and large peak somewhere within a ∼150 cm^{-1} range about the cited values, it is of little diagnostic value without modeling.

Much more definitive bands are the weaker, narrower peaks that were observed at 711.3 ± 1.0 cm^{-1} (ν_4 CO_3^{2-} degenerate-in-plane bend, ordinary, fwhm = 7 cm^{-1}) and 873.9 ± 2.7 cm^{-1} (ν_2 CO_3^{2-} symmetric out-of-plane bend, extraordinary, fwhm = 15 cm^{-1}) as measured by us with 99.9% pure $CaCO_3$. Common minerals and an XRF study of dust from a bookshelf next to the room where these dust samples were collected[72] suggest that Ca, Mg, and Fe are the most important cations for our carbonate dust with a minor contribution from Mn (the Kα signal for Fe was 68 times larger than Mn). Lane and Christensen[84] made measurements on various metal carbonates and have shown that a plot of the peak positions of ν_4 vs ν_2 is diagnostic for the cation. A search of the library of individual dust spectra found 18 spectra out of 63 that had narrow peaks in the vicinity of both ν_4 and ν_2 of carbonate. The frequencies are presented on a ν_4 vs ν_2 plot in Figure 5 (filled circles) along with our own measurements of pure $CaCO_3$ (down pointing empty triangles) and dust scraped from dolomite rock (empty circles). Trends analyzed and extracted from the work of Lane and Christensen for $CaCO_3$ (calcite), $Ca_{0.5}Mg_{0.5}CO_3$ (dolomite), $MgCO_3$ (magnesite), and $Fe_{0.88}Mn_{0.05}Mg_{0.07}CaO_3$ (as close as they could get to siderite, $FeCO_3$) have been shifted to the average of our $CaCO_3$ observations and presented as dotted lines. These trends represent the IR spectroscopic analogue of an assemblage triangle as used in geology[85] to indicate solution compositions or phases that can be synthesized or observed.[86] The ellipse at the bottom of the diagram shows 10 particles (d1, d9, d25, d31, d33, d36, d50, d56, d60, and d63) out of 63 that can be considered to be from calcitic limestones, calcite with a small amount of Mg doping (less than 10%). The average value of ν_4 for this group is 713.4 ± 1.8 cm^{-1} (as shifted along the Ca−Mg replacement line from 711.3 ± 1.0 cm^{-1} for pure calcite) and implies about 6.5 mol % Mg or a formula of $Ca_{0.93}Mg_{0.07}CO_3$ on average. Mg is the most likely impurity since most carbonate skeletons of marine organisms (like seashells) have variable amounts of Mg (up to 50%).[87] Another ellipse (above the first) encircles a region where dolomite (at right) changes into ankerite ($Ca_{0.5}Fe_{0.5}CO_3$) at left. This region is indicated by our IR estimate of the Fe/Mn−Mg replacement line (dotted, nearly horizontal line). The three dust particles closest to dolomite (d13, d27, and d48) have ν_2 = 881.6 ± 0.6 cm^{-1} which is red-shifted 4.5 cm^{-1} from pure dolomite (886.1 cm^{-1}) suggesting ∼13 mol % Fe or an average composition of $Ca_{0.5}Mg_{0.37}Fe_{0.13}CO_3$. Likewise, the group of 4 ankerite particles to the left of the dolomites (d4, d14, d19, and d29) have ν_2 = 875.9 ± 0.6 cm^{-1} which is red-shifted by 10.2 cm^{-1} from pure dolomite suggesting ∼29 mol % Fe or $Ca_{0.5}Mg_{0.21}Fe_{0.29}CO_3$. The narrow CO_3^{2-} bends are quite sensitive to composition.

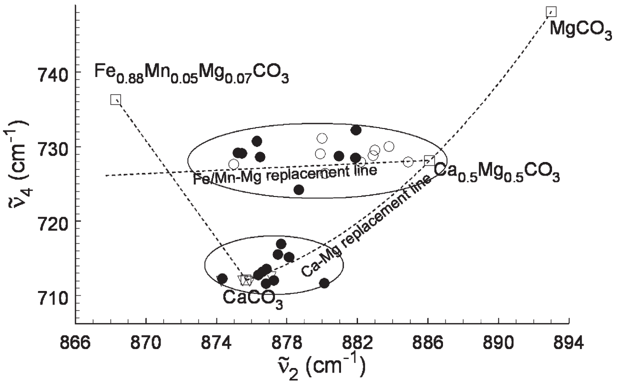

Figure 5. Plot of the CO_3^{2-} $\tilde{\nu}_4$ band position vs the $\tilde{\nu}_2$ band postion revealing the composition of the carbonates. The filled circles are carbonates from the library of 63 dust particles, the open circles are particles scraped from dolomite rock, and the open triangles are pure $CaCO_3$ particles—all trapped in mesh holes. The open squares are calibrating results from Lane and Christensen which have been offset so that the two pure $CaCO_3$ sets overlap. This presentation is the infrared analogue to a Fe−Ca−Mg carbonate assemblage diagram where the dotted lines represent substitution of one metal for another.

Figure 6 shows spectra of carbonate containing particles of limestone, dolomite, and ankerite. The line shapes of the strong ν_3 CO_3^{2-} antisymmetric stretch band in many of the Figure 6 spectra suggest that the Mg doping of the limestone, Fe doping of

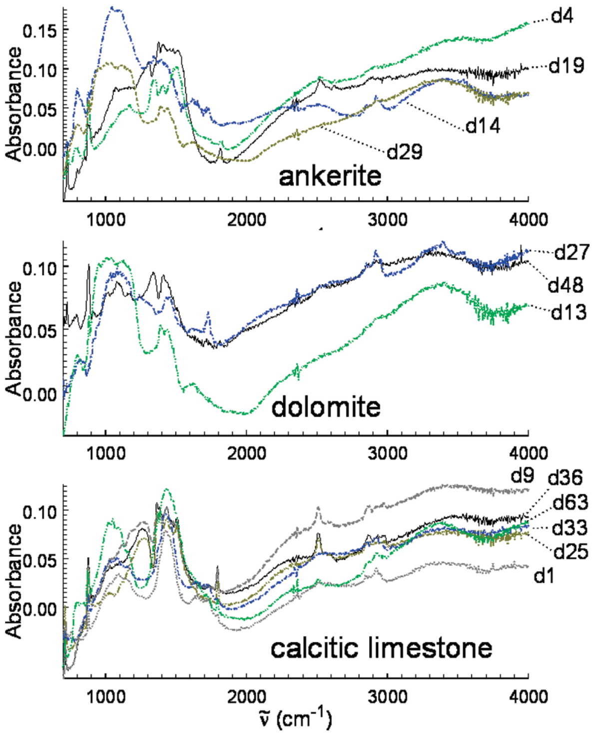

Figure 6. Selected plots of individual particles from three carbonate groups including calcitic limestone (Mg-doped calcite), dolomite (Fe-doped $Mg_{0.5}Ca_{0.5}CO_3$), and ankerite (Mg-doped $Fe_{0.5}Ca_{0.5}CO_3$). Big peaks in some spectra around 1000 cm^{-1} are not carbonate. The largest carbonate peak near 1425 cm^{-1} is saturating for particles of this size and is often split due to doping.

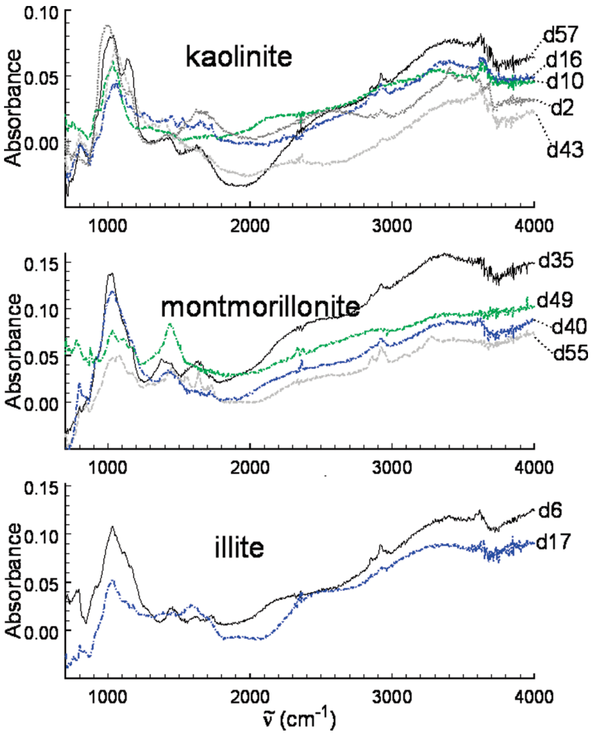

Figure 7. Typical spectra of particles dominated by clay, including types we have grouped into kaolinite, montmorillonite, and illite. The kaolinite structure is more ordered and has only OH^- features, while the other two clays have much cation substitution and both OH^- and H_2O features.

the dolomites, or Mg doping of the ankerites can produce a splitting of this band. It would be interesting to look for a correlation of the magnitude of the splitting with the intensity of doping. These carbonate dust spectra often exhibit the $\nu_1 + \nu_4$ combination band as a fairly narrow peak; it occurs at 1793.8 ± 0.5 cm^{-1} with pure $CaCO_3$ and 1817 cm^{-1} in Fe-doped dolomite rock dust and may prove to be as useful as ν_4 and ν_2 in elucidating various metal compositions. There also exist other overtones and/or combination bands in the regions of 2507−2523 cm^{-1} (2509.8 ± 0.7 cm^{-1} in pure $CaCO_3$), 2848−2873 cm^{-1} (2872 ± 3 cm^{-1} in pure $CaCO_3$), and 2924−2980 cm^{-1} (2982.1 ± 0.6 cm^{-1} in pure $CaCO_3$) which need to be accounted for if one is interested in characterizing the organic material from the overlapping CH stretching region.

Using the simultaneous appearance of ν_2, ν_3, and ν_4 carbonate bands as the criteria, at least 27% of the particles are found to have carbonate, including 16% with calcitic limestone (light Mg doping), 5% with light Fe doping of dolomite, and 6% that might be called ankerite (heavy Fe doping of dolomite or light Mg doping of ankerite).

Clays. Clays (layered aluminosilicates) are evident in the spectra, but there are a wide variety of clays. So, these spectra were considered in terms of three major types: kaolinite, montmorillonite, and illite. Characteristic dust particle spectra of these types of clay are given in Figure 7. Clays are generally trirefringent, so their spectra are mixtures of variable amounts of X ($E||a$), Y ($E||b$), and Z ($E||c$) spectra. Their spectra are dominated by intense peaks of variable broadness in the 900−1120 cm^{-1} range and two types of OH stretch bands, including broad, H-bonded bands due to H_2O and narrow OH^- bands. Three specific clays of these three types were acquired from the Clays Repository (www.clays.org). Kaolinite [$Al_2Si_2O_5(OH)_4$] is the most ordered structure of the clays exhibiting fairly narrow bands across its IR spectrum. Using kaolinite sample KGa-1b from Washington Co. Georgia, the average spectra of 3 different 5 μm particles trapped in mesh holes gave strong peaks at 916, 940, 1011, 1042, and 1117 cm^{-1}, very sharp OH^- peaks at 3617, 3651, 3665, and 3690 cm^{-1}, no H_2O stretch bands, weaker, but characteristic, bands at 705, 759, and 849 cm^{-1}, as well as small quartz-like bands. Because so many other minerals have strong bands in the 900−1120 cm^{-1} range, it is the sharp (~12 cm^{-1} fwhm) OH^- peaks that are most distinctive for kaolinite. A total of 8 particles (d2, d10, d16, d43, d47, d50, d54, and d57) out of 63 have a set of sharp OH^- bands and strong (but possibly obscured) bands in both the 916−940 and 1000−1120 cm^{-1} ranges. The top part of Figure 7 shows a selection of dust particle spectra with the strongest kaolinite components.

Montmorillonite [$(Na,Ca)_{0.33}(Al,Mg)_2Si_4O_{10}(OH)_2 \cdot nH_2O$] and illite [$(K,H_3O)(Al,Mg,Fe)_2(Si,Al)_4O_{10}[(OH)_2,(H_2O)]$] represent a large set of clays with a variety of cation substitutions causing broader OH^- bands and a combination of OH^- and H_2O stretching vibrations. Calibration spectra of the three repository clays were recorded both with a diamond ATR instrument and as 5 μm particles in mesh holes.[72] While the ATR and 5 μm particle spectra of kaolinite (KGa-1b) have similar peaks throughout the range, the montmorillonite (STx-1b from Gonzales Co. Texas) and illite (IMt-1, cambrianshale from Silver Hill Montana) both notably have their main peaks considerably blue-shifted and broadened from the diamond ATR spectrum

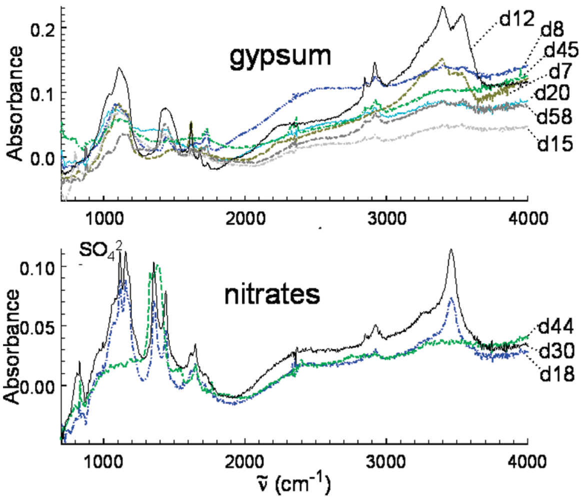

Figure 8. Plot with seven particles dominated by gypsum (top) and a plot with three nitrate particles (bottom). Particle d44 is dominated by $NaNO_3$, while particles d18 and d30 are mixtures of $Ca(NO_3)_2$ and $CaSO_4$.

values. Comparative differences between diamond ATR and single-particle mesh spectra (for the same material) afford a good indication of the presence of important Mie effects. In fact, the strongest bands of quartz, carbonates, and montmorillonite/illite clays all show such effects for 5 μm diameter particles. The spectrum of 5 μm diameter montmorillonite has its most intense peak at 1051 cm^{-1}, while the diamond ATR spectrum is dominated by a peak at 998 cm^{-1} which agrees with the ATR work of Jung et al.,[88] so there is a 53 cm^{-1} blue shift due to particle size or shape. The 5 μm diameter montmorillonite particles show small peaks at 799, 842, 917 cm^{-1}, a main peak at 1051 with a shoulder near 1120 cm^{-1} (~80 cm^{-1} fwhm), and an OH stretching region with a very broad peak at ~3408 cm^{-1} due to H_2O and a peak at 3623 cm^{-1} (fwhm = 52 cm^{-1}) due to OH^- (broader than kaolinite, but much narrower than H_2O in clay). Particles d35, d39, d40, d49, d55, and d63 may have montmorillonite contributions. Our illite repository clay (IMt-1) shows similar behavior with a main peak at 1030 cm^{-1} which occurs at 958 cm^{-1} in the ATR spectrum of the same material. The 5 μm diameter illite particle shows a small peak at 834 cm^{-1}, a main peak at 1030 cm^{-1} (blue-shifted by 72 cm^{-1} from the ATR spectrum), and an OH^- peak at 3614 cm^{-1}. Particles d6, d17, and d56 may have some illite contributions. Note that the repository clays often have some organic material detected in the IR spectra, as do the dust particles. Tentatively, about 9 out of 63 particles have illite/montmorillonite IR signatures. It is hard to definitively distinguish the montmorillonite and illite particles, but representative dust particle spectra are given in the bottom two panels of Figure 7. The occurrence of all three clay types is ~17 particles out of 63, or 27% of the particles.

Sulfate. Gypsum, $CaSO_4 \cdot 2H_2O$, is a soft, somewhat soluble, and trirefringent mineral that occurs naturally and is used in dry wall materials for the construction of homes. The spectra of gypsum-dominated dust particles are given in the top of Figure 8. The most intense peak is a band (ν_3 stretch) of SO_4 that occurs within the range of 1108−1135 cm^{-1} whether the polarization is along the *a*, *b*, or *c* crystal axes. It is not as intense as the main peak of quartz or carbonate; thus, much less line shape distortion is expected for 5 μm diameter gypsum particles. There are also distinctive, narrow, water bending bands at 1620 cm^{-1} ($E||c$) and 1684 cm^{-1} ($E||b$) and water OH stretches at 3244, 3398 ($E||c$), 3486, and 3559 cm^{-1} ($E||b$). Particles d2, d6, d7, d8, d12, d15, d20, d27, d32, d45, d54, d57, d58, and d61 appear to have gypsum components amounting to 14 out of 63 particles or an occurrence in 22% of the particles. Also, several particles (d18 and d30) have some sulfate mixed with $Ca(NO_3)_2$ and are discussed in the next section.

Nitrates. Nitrates are evident in particles d18, d30, and d44 (see Figure 8 bottom). Particle d44 shows narrow peaks at 834 and 1766 cm^{-1}, a dominant band with peaks at 1330 and 1383 cm^{-1} (which average to 1357 cm^{-1}), and weaker bands at 1653 and 2400 cm^{-1}. This matches the nitrate bands of $NaNO_3$ very well: the ν_2 is very sensitive to the cation and occurs at 836 cm^{-1}, the ν_3 is strong and broad occurring at 1358 cm^{-1}, and the $\nu_1 + \nu_4$ is narrow occurring at 1767 cm^{-1}.[89] The spectra of d18 and d30 (bottom of Figure 8) are very similar to each other and contain both nitrate and sulfate features with peaks at 831 cm^{-1}, a split pair at 1116 and 1154 cm^{-1}, another split pair at 1356 and 1440 cm^{-1}, and 1648 and 3456 cm^{-1}. The nitrate ν_3 band splits with certain perturbations (like multiply charged cations and/or hydrates), and the observed 84 cm^{-1} splitting best matches the 80 cm^{-1} literature splitting of $Ca(NO_3)_2$. By comparison, this splitting[89] is 50 cm^{-1} with NH_4NO_3 which might be present in lesser amounts or with broader peaks. Most of the observed d18 and d30 peak positions and intensities compare well to $Ca(NO_3)_2$ literature values[89] as given in parentheses in the following list: 831 (821), 1356 (1350), 1440 (1430), 1648 (1640), and 3456 (3450) cm^{-1}. The particles d18 and d30 also have sharp sulfate peaks at 1116 and 1154 cm^{-1} (a splitting of 38 cm^{-1}) which are different than the single peak of sodium or potassium sulfate.[89] This is also different than gypsum (single broad peak at 1130 cm^{-1})[89] or $(NH_4)_2SO_4$ (single broad peak at 1105 cm^{-1})[89] which could be present in lesser amounts or with broader peaks. The splitting of 38 cm^{-1} matches (in both line shape and peak position) anhydrous $CaSO_4$ (as judged by the NIST Webbook IR spectrum), which is a bit surprising as these particles were not dried beyond that of the capture process. So particles d18 and d30 might be tentatively identified as containing $Ca(NO_3, SO_4)$, which is very interesting because $CaCO_3$ dust particles are known to react with atmospheric NO_x and SO_x[90] producing $Ca(NO_3, SO_4)$ particles. Including particles d39 and d43, which may have a smaller amount of nitrate, 5 out of 63 particles have nitrate in general which is an occurrence in 8% of the particles.

Organics. Organics, as judged by the pair of asymmetric and symmetric aliphatic $-CH_2-$ stretches, usually with ~2:1 intensity, were observed in a minimum of 40 out of 63 particles (d1, d2, d5, d8, d11, d12, d14, d15, d16, d18, d20, d21, d22, d23, d26, d27, d28, d30, d31, d32, d33, d34, d35, d37, d39, d40, d45, d46, d47, d48, d50, d53, d54, d55, d57, d58, d60, d61, d62, d63). A histogram of the occurrence of peaks in the CH stretching region is given in Figure 9 (bottom). The peaks at 2850.8 ± 0.3 and 2920.4 ± 0.5 cm^{-1} (as fit with a nonlinear least-squares routine giving the solid line) have similar occurrences, which is consistent with them being a pair of symmetric and asymmetric aliphatic methylene stretches. The smaller distributions at 2867, 2932, 2952, and 2970 cm^{-1} are likely $-CH_3$ bands that occur less often (3:8 ratio to methylenes). It is interesting to compare the average spectrum of the 63 particles in the same region (Figure 9 top) to the histogram. In fact, almost every individual particle spectrum has more explicit information than the average spectrum which is analogous to bulk spectra of dust, hence the utility of recording individual particle spectra. Much of our approach to analysis was

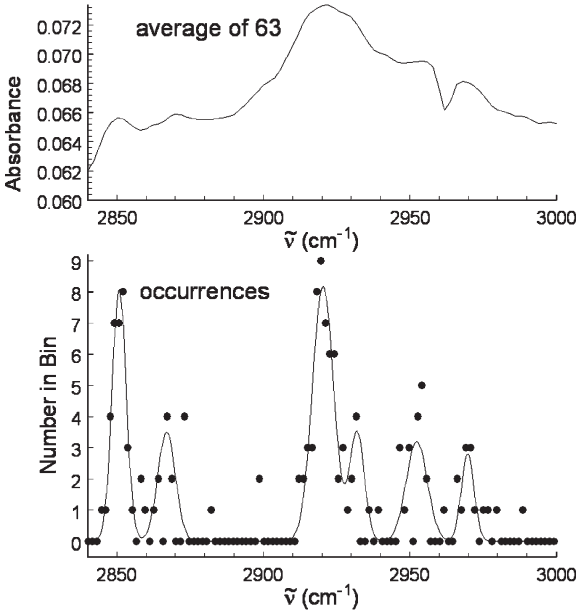

Figure 9. Plot of the average of the 63 dust particle spectra in the CH stretching region (top); histogram from the list of peaks in the same region (bottom). The histograms were fit to Gaussian distributions which show that the methylene peaks at 2850.8 ± 0.3 and 2920.4 ± 0.5 cm^{-1} are correlated and that they occur more frequently than the smaller methyl peaks.

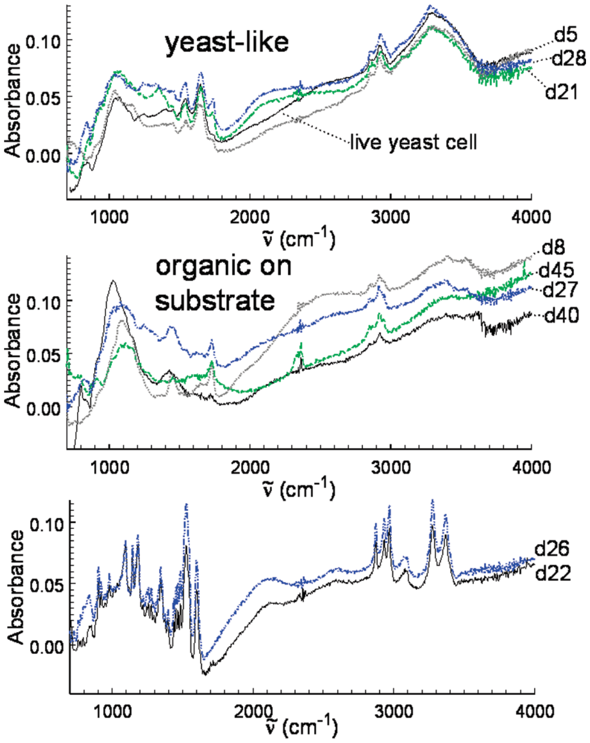

Figure 10. Spectra of typical groups of particles with organic material as primarily evident by peaks in the CH stretching region. Particles with spectra similar to a live yeast cell are shown on the top. In the middle are typical spectra with organic material, including a band at ~1730 cm^{-1}, on some substrate such as clay. On the bottom are two particles that have the spectra of a synthetic organic reagent.

guided by the IR bulk dust studies of Hobert[76] who could not correlate any other peaks with the $-CH_2-$ stretches in the bulk spectra, but almost every individual spectrum with organics has multiple peaks that are clearly correlated with the $-CH_2-$ stretches. Some of the particles (d5, d21, d23, d28, and d62) have organic contributions that are similar to that of a live yeast cell[74] (or recently living material) as shown at the top of Figure 10. Note the occurrence of a small peak at ~1730 cm^{-1} (often assigned to the ester linkage of phospholipids of membranes), and bigger peaks at ~1650 cm^{-1} (protein amide I band) and ~1542 cm^{-1} (the protein amide II band). There was also another group (d8, d27, d40, and d45) that had a bigger peak at ~1730 cm^{-1} than the amide I and II bands (if they occurred at all), which were attached to clay or gypsum particles. We suspect that such spectra represent some step along the decomposition of organic material on mineral particles, and models are being developed to separate the organic spectra from that of the mineral substrates. There seems to be a reasonable chance of extracting a progression from almost-living organic material to humus. Finally, there were two particles (d22 and d26) with very similar spectra with characteristics of small organic molecules. There is similarity to the spectra of simpler known compounds: the fingerprint region matches nitrobenzene, there are aliphatic and aromatic C—H stretches, and the aliphatics appear to have a butyl intensity pattern with an amide group. The spectra are suggestive of a butylamine in the para position of a nitrobenzene, but more work is required before a definitive assignment can be made. The $-NO_2$ and $-NH_2$ groups possibly suggest synthetic or manmade molecules (as might be found in a chemistry department), although more work is needed.

Rising Basline Issue. Almost every individual spectrum in the dust library of 63 has a baseline that rises with increasing wavenumber (readily evident in Figures 4, 6, 7, 8, and 10) on a scale evident relative to the size of vibrational features. While it is possible to get a monotonically rising baseline with Mie theory (by adding a nonzero imaginary component to the constant part of the complex dielectric function[72]), such a feature would also be seen in the ATR powder spectra of calibrating dust components, but it is not.[72] Furthermore, Mie theory never mimicked the qualitative shape of the rising baselines. It is our opinion that this baseline rise is due to a lensing effect of the roughly globular dust particles. A spherical particle has a focal point just outside of its diameter. From geometrical optics it is known that the stronger the real part of the sphere's index of refraction, the closer the focal point is to the sphere and, therefore, a lesser amount of light hits the detector. Similar behavior can be expected for globular dust particles. Generally, one can expect a rise of the real part of the index of refraction with increasing wavenumbers, away from strong vibrations, as is apparent by the leading term in the derivative of Cauchy relations[91] with respect to wavenumbers. For a specific example, note that the real part of the index of refraction of fused quartz[92] rises from 1.407 at 2851 cm^{-1} to 1.433 at 4300 cm^{-1} and this corresponds to a region of rising background in the experimental dust data (see Figure 4). Therefore, we suspect that the rising baselines with increasing wavenumbers are due to a lensing effect of the particles, although more work would be needed to demonstrate this assertion.

■ CONCLUSION

The occurrences of components of dust have been determined with the statistics offered by 63 particles. Most of the spectra of

Table 1. Summary of Component Occurences

component	formula	no. particles out of 63	% occurence
quartz	SiO_2	34	54
calcitic limestone	$Ca_{0.93}Mg_{0.07}CO_3$	10	16
dolomite	$Ca_{0.50}Mg_{0.37}Fe_{0.13}CO_3$	3	5
ankerite	$Ca_{0.50}Mg_{0.21}Fe_{0.29}CO_3$	4	6
total carbonates	XCO_3	17	27
gypsum	$CaSO_4 \cdot 2H_2O$	14	22
kaolinite	$Al_2Si_2O_5(OH)_4$	8	13
montmorillonite/illite	$(Na,Ca)_{0.33}(Al,Mg)_2Si_4O_{10}(OH)_2 \cdot nH_2O$	9	14
organics	$X{-}CH_2{-}Y$	40	63
calcium nitrate/sulfate	$Ca(NO_3, SO_4)$	2	3
sodium nitrate	$NaNO_3$	1	2
total nitrates	XNO_3	5	8

individual dust particles are mixtures of two or more components, although a few have many components. As a result, it is easier to see definitive features of components in the individual spectra. Many sharp peaks are observed in the individual spectra that are averaged away in bulk dust spectra (dust pressed into KBr pellets). The individual particle spectra show information about the crystalline nature and orientation of particle components which can begin to be extracted with calibrating measurements on particles of the pure components.

A summary of occurrences for those substances that have so far been identified in the dust is presented in Table 1. Quartz is the most common mineral occurring in 54% of the particles, carbonates are observed in 27%, clays in 27%, gypsum in 22%, and nitrates in 8% of the particles. Organics were detected in 63% of the particles, and the fraction varies from a subset that seems entirely organic to most that have organics stuck to or within mineral substrates. It is very difficult to detect any other organic peaks in a bulk dust spectrum other than the CH_2 stretches;[76] however, the individual spectra reveal a variety of other organic peaks enabling a more detailed characterization of the organics. It appears possible to extract a sequence of spectra that follows the decomposition of live organic material on dust particles, but this will be the topic of a future paper.

The narrow ν_2 and ν_4 bending bands of carbonate have enabled the construction of an IR spectroscopy equivalent of a three-component assemblage diagram (Figure 5) as might be used in geology or inorganic chemistry. This work suggests that the carbonates are divided into calcitic limestone (<10% Mg doping), dolomite (~13% Fe doping), and ankerite (~21% Mg doping). The narrow carbonate peaks, which get averaged-away in bulk spectra, can be quite revealing about the metal composition of individual carbonate particles and the sample at large. Finally, the splitting of the strong carbonate ν_3 band might be used to give the doping of individual particles with a supporting calibration study.

Clearly there are many other components in the dust particle spectra that remain to be discovered. With individual spectra, the issue becomes one of the probability of finding a minority component dominated particle, i.e., the size of the library, as opposed to bulk studies which involve seeing a minority spectral feature above the noise of the bulk spectrum in a forest of stronger peaks. The ability to record the IR spectra of a large number of particles is important.

The chemical identity of airborne dust particles is of much interest in health fields. For example, it has been found that respired graphitic nanoparticles can end up in the olfactory bulb of mouse brains whereas metal nanoparticles do not.[93] Since microparticles may be more reflective of the local environment, it is quite significant that there exists a second distribution in the 1−10 μm region in the deposition fraction vs particle size in data from the mouse alveolar region. Clearly, a chemical evaluation of microparticles is important.

While particles of ~3−5 μm size are important in health, they are also interesting from a spectroscopic standpoint. Noting that the current data set carefully preserves intensity information, the data can be directly modeled with Mie theory using scaling factors from previous work.[40,54,73,74] Many of the strongest bands of the common components like quartz, carbonate, and clay have one band with a cross section that is bigger than the physical cross section of the particle. This means that there will be many interesting saturation effects which will result in peak shifting, broadening, or even breaking into multiple peaks. Evidence of bi- or trirefringence abounds in the data. It is a general difficulty in the interpretation of dust particle spectra because the spectral peaks will change intensity with different orientations. Multiple calibration spectra of pure component particles will be required to sort through this effect, but it is approachable and the subject of a following paper. The individual spectra are of sufficient quality that overtone and combination bands are readily observed. These features overlap with the important CH stretching region of organic components, and there is much less literature information on such bands, so again calibration work will be needed.

The most important information to be extracted still lies ahead. The individual spectra can be modeled with a combination of Mie theory and Bruggeman effective medium theory.[72] This requires the recording of spectra of pure 5 μm particles in mesh of all the important components found in the dust library. Once these spectra are fit to a Mie model, the results can be combined with Bruggeman effective medium theory to model the spectra of particles with combinations of components. One obtains the volume fractions of each component which is a more quantitative assessment than the occurrences of this work. These results will be reported in a following paper. Finally, we have made all 63 individual spectra and the peak list available in the Supporting Information so that others may begin to model the data.

■ ASSOCIATED CONTENT

Ⓢ Supporting Information. Digital trace and peak position of all 63 individual spectra. This material is available free of charge via the Internet at http://pubs.acs.org.

■ ACKNOWLEDGMENT

We thank the National Science Foundation for support of this work under grant numbers CHE 0848486 and CHE-0639163.

■ REFERENCES

(1) Holmes, H. *The Secret Life of Dust: From the Cosmos to the Kitchen Counter, the Big Consequences of Little Things*; John Wiley & Sons: New York, 2001.

(2) Wopenka, B.; Swan, P. D. *Mikrochim. Acta* **1988**, *1*, 183.

(3) Sandford, S. A.; Walker, R. M. *Astrophys. J.* **1985**, *291*, 838.

(4) Flynn, G. J. *Planetary Space Sci.* **1994**, *42*, 1151.

(5) Hess-Kosa, K. *Indoor Air Quality: Sampling Methodologies*; CRC Press: Boca Raton, FL, 2002.

(6) Hertel, O.; Goodsite, M. E. Urban air pollution climates throughout the world. In *Air Quality in Urban Environments*; Royal Society of Chemistry: London, 2009; Vol. 28, p 1.

(7) Husar, R. B. Intercontinental transport of dust: Historical and recent observational evidence. In *Intercontinental Transport of Air Pollution*; Stohl, A., Ed.; Springer-Verlag: Berlin. 2004; Vol. 4-G, pp 227.

(8) Prather, K. A. *ChemSusChem* **2009**, *2*, 377.

(9) Georgakopoulos, D. G.; Despres, V.; Froelich-Nowoisky, J.; Psenner, R.; Ariya, P. A.; Posfai, M.; E., A. H.; Moffett, B. F.; Hill, T. C. J. *Biogeosciences* **2009**, *6*, 721.

(10) Hladil, J.; Strnad, L.; Salek, M.; Jankovska, V.; Simandl, P.; Schwarz, J.; Smolik, J.; Lisa, L.; Koptikova, L.; Rohovec, J.; Boehmova, V.; Langrova, A.; Kocianova, M.; Melichar, R.; Admovic, J. *Bull. Geosci.* **2008**, *83*, 175.

(11) Reheis, M. C.; Buadahn, J. R.; Lamothe, P. J.; Reynolds, R. L. *J. Geophys. Res.* **2009**, *114*, F01028.

(12) Cole, J. M.; Goldstein, S. L.; deMenocal, P. B.; Hemming, S., R.; Grousset, F., E. *Earth Planet. Sci. Lett.* **2009**, *278*, 257.

(13) Moreno, T.; Amato, F.; Querol, X.; Alastuey, A.; Elvira, J.; Gibbons, W. *Environ. Geol.* **2009**, *57*, 411.

(14) Polichetti, G.; Cocco, S.; Spinali, A.; Trimarco, V.; Nunziata, A. *Toxicology* **2009**, *261*, 1.

(15) Michaels, R. A.; Kleinman, M. T. *Aerosol Sci. Technol.* **2000**, *32*, 93.

(16) Hoefner, S. *Dust Formation and Winds around Evolved Stars: The Good, the Bad, and the Ugly Cases*; Cornell University Library: Ithaca, NY, 2009.

(17) Natta, A. *Phys. Scr.* **2008**, *T130*, 014014 (6 pp).

(18) Mennella, V. *J. Phys.: Conf. Ser.* **2005**, *6*, 197.

(19) Eastwood, P. *Particulate Emissions from Vehicles*; John Wiley & Sons: Chichester, England; Hoboken, NJ, 2008.

(20) Dunder, T.; Miller, R. E. *J. Chem. Phys.* **1990**, *93*, 3693.

(21) Christiansen, C. *Ann. Phys.* **1884**, *259*, 298.

(22) Dumas, P.; Carr, G. L.; Williams, G. P. *Analusis* **2000**, *28*, 68.

(23) Raynal, P. I.; Quirico, E.; Borg, J.; Deboffle, D.; Dumas, P.; d 'Hendecourt, L.; Bibring, J. P.; Langevin, Y. *Planetary Space Sci.* **2000**, *48*, 1329.

(24) Coe, J. V.; Heer, J. M.; Teeters-Kennedy, S.; Tian, H.; Rodriguez, K. R. *Annu. Rev. Phys. Chem.* **2008**, *59*, 179.

(25) Coe, J. V.; Rodriguez, K. R.; Teeters-Kennedy, S.; Cilwa, K.; Heer, J.; Tian, H.; Williams, S. M. *J. Phys. Chem. C* **2007**, *111*, 17459.

(26) Ebbesen, T. W.; Lezec, H. J.; Ghaemi, H. F.; Thio, T.; Wolff, P. A. *Nature (London, U.K.)* **1998**, *391*, 667.

(27) Genet, C.; Ebbesen, T. W. *Nature (London, U.K.)* **2007**, *445*, 39.

(28) Garcia-Vidal, F. J.; Martin-Moreno, L.; Pendry, J. B. *J. Opt. A: Pure. Appl. Opt.* **2005**, *7*, S97.

(29) Fang, N.; Zhang, X. *Appl. Phys. Lett.* **2003**, *82*, 161.

(30) Fang, N.; Liu, Z.; Yen, T.-J.; Zhang, X. *Opt. Express* **2003**, *11*, 682.

(31) Degiron, A.; Lezec, H. J.; Yamamoto, N.; Ebbesen, T. W. *Opt. Commun.* **2004**, *239*, 61.

(32) Barnes, W. L.; Dereux, A.; Ebbesen, T. W. *Nature (London, U.K.)* **2003**, *424*, 824.

(33) Zhang, D.; Wang, P.; Jiao, X.; Tang, L.; Lu, Y.; Ming, H. *Wuli* **2005**, *34*, 508.

(34) Martin-Moreno, L.; Garcia-Vidal, F. J. *Adv. Solid State Phys.* **2004**, *44*, 69.

(35) Moller, K. D.; Farmer, K. R.; Ivanov, D. V. P.; Sternberg, O.; Stewart, K. P.; Lalanne, P. *Infrared Phys. Technol.* **1999**, *40*, 475.

(36) Ulrich, R. Modes of Propagation on an Open Periodic Waveguide for the Far Infrared. *Optical and Acoustical Micro-electronics*; Polytechnic Press of the Polytechnic Institute of New York; Brooklyn, NY, 1974.

(37) Popov, E.; Neviere, M.; Enoch, S.; Reinisch, R. *Phys. Rev. B: Condens. Matter Mater. Phys.* **2000**, *62*, 16100.

(38) Ghaemi, H. F.; Thio, T.; Grupp, D. E.; Ebbesen, T. W.; Lezec, H. J. *Phys. Rev. B: Condens. Matter Mater. Phys.* **1998**, *58*, 6779.

(39) Barnes, W. L.; Murray, W. A.; Dintinger, J.; Devaux, E.; Ebbesen, T. W. *Phys. Rev. Lett.* **2004**, *92*, 107401.

(40) Heer, J.; Corwin, L.; Cilwa, K.; Malone, M. A.; Coe, J. V. *J. Phys. Chem. C* **2010**, *114*, 520.

(41) Williams, S. M.; Stafford, A. D.; Rodriguez, K. R.; Rogers, T. M.; Coe, J. V. *J. Phys. Chem. B* **2003**, *107*, 11871.

(42) Williams, S. M.; Stafford, A. D.; Rogers, T. M.; Bishop, S. R.; Coe, J. V. *Appl. Phys. Lett.* **2004**, *85*, 1472.

(43) Williams, S. M.; Rodriguez, K. R.; Teeters-Kennedy, S.; Stafford, A. D.; Bishop, S. R.; Lincoln, U. K.; Coe, J. V. *J. Phys. Chem. B* **2004**, *108*, 11833.

(44) Williams, S. M.; Coe, J. V. *Plasmonics* **2006**, *1*, 87.

(45) Williams, S. M.; Rodriguez, K. R.; Teeters-Kennedy, S.; Shah, S.; Rogers, T. M.; Stafford, A. D.; Coe, J. V. *Nanotechnology* **2004**, *15*, S495.

(46) Rodriguez, K. R.; Shah, S.; Williams, S. M.; Teeters-Kennedy, S.; Coe, J. V. *J. Chem. Phys.* **2004**, *121*, 8671.

(47) Coe, J. V.; Williams, S. M.; Rodriguez, K. R.; Teeters-Kennedy, S.; Sudnitsyn, A.; Hrovat, F. *Anal. Chem.* **2006**, *78*, 1384.

(48) Teeters-Kennedy, S.; Williams, S. M.; Rodriguez, K. R.; Cilwa, K.; Meleason, D.; Sudnitsyn, A.; Hrovat, F.; Coe, J. V. *J. Phys. Chem. C* **2007**, *111*, 124.

(49) Rodriguez, K. R.; Tian, H.; Heer, J. M.; Coe, J. V. *J. Phys. Chem. C* **2007**, *111*, 12106.

(50) Rodriguez, K. R.; Tian, H.; Heer, J. M.; Teeters-Kennedy, S.; Coe, J. V. *J. Chem. Phys.* **2007**, 126.

(51) Teeters-Kennedy, S. M.; Rodriguez, K. R.; Rogers, T. M.; Zomchek, K. A.; Williams, S. M.; Sudnitsyn, A.; Carter, L.; Cherezov, V.; Caffrey, M.; Coe, J. V. *J. Phys. Chem. B* **2006**, *110*, 21719.

(52) Coe, J. V.; Williams, S. M.; Rodriguez, K. R. Coated Biperiodic Metallic Mesh Arrays with Molecular Monolayers and Lipid Bilayers Thereon. U.S. Patent 6,863,991, March 8, 2005; The Ohio State University, Columbus, OH, 2005; 16 pp.

(53) Coe, J. V.; Williams, S. M. Method for Uniform Electrochemical Reduction of Apertures to Micron and Submicron Dimensions Using Commercial Biperiodic Metallic Mesh Arrays and Devices Derived Therefrom. U.S. Patent 6,797,405, Sept. 28, 2004; The Ohio State University, Columbus, OH, 2004; 20 pp.

(54) Cilwa, K. E.; Rodriguez, K. R.; Heer, J. M.; Malone, M. A.; Corwin, L. D.; Coe, J. V. *J. Chem. Phys.* **2009**, *131*, 061101.

(55) Glass, N. E.; Maradudin, A. A.; Celli, V. *Phys. Rev. B: Condens. Matter Mater. Phys.* **1983**, *27*, 5150.

(56) Kneipp, K.; Kneipp, H.; Manoharan, R.; Hanlon, E. B.; Itzkan, I.; Dasari, R. R.; Feld, M. S. *Appl. Spectrosc.* **1998**, *52*, 1493.

(57) Brolo, A. G.; Arctander, E.; Gordon, R.; Leathem, B.; Kavanagh, K. *Nano Lett.* **2004**, *4*, 2015.

(58) Dintinger, J.; Klein, S.; Ebbesen, T. W. *Adv. Mater. (Weinheim, Ger.)* **2006**, *18*, 1267.

(59) Coe, J. V.; Williams, S. M.; Rodriguez, K., R.; Teeters-Kennedy, S.; Sudnitsyn, A.; Hrovat, F. *Anal. Chem.* **2006**, *78*, 1384.

(60) Murphy, D. M.; Cziczo, D. J.; Froyd, K. D.; Hudson, P. K.; Matthew, B. M.; Middlebrook, A. M.; Peltier, R. E.; Sullivan, A.; Thomson, D. S.; Weber, R. J. *J. Geophys. Res., [Atmos.]* **2006**, 111.

(61) Thomson, D. S.; Schein, M. E.; Murphy, D. M. *Aerosol Sci. Technol.* **2000**, *33*, 153.

(62) Murphy, D. M.; Thomson, D. S. *Aerosol Sci. Technol.* **1995**, *22*, 237.

(63) Flynn, G. J.; Keller, L. P.; Wirick, S.; Jacobsen, C.; Sutton, S. R. *J. Phys. IV* **2003**, *104*, 367.

(64) Flynn, G. J.; Keller, L. P.; Jacobsen, C.; Wirick, S. *Meteorit. Planet. Sci.* **1999**, *34*, A36.

(65) Johansso, S. A. E. *Analyst (Cambridge, U.K.)* **1992**, *117*, 259.

(66) Laskin, A.; Cowin, J. P.; Iedema, M. J. *J. Electron Spectrosc. Relat. Phenom.* **2006**, *150*, 260.

(67) Widmann, J. F.; Aardahl, C. L.; Davis, E. J. *TrAC Trends Anal. Chem.* **1998**, *17*, 339.

(68) Wopenka, B. *Earth Planet. Sci. Lett.* **1988**, *88*, 221.

(69) Dominici, F.; McDermott, A.; Zeger, S. L.; Samet, J. M. *Environ. Health Persepect.* **2003**, *111*, 39.

(70) Hinds, W. C. *Aerosol Technology: Properties, Behavior, and Measurement of Airborne Particles*; John Wiley: New York, 1982.

(71) Kaiser, J. *Science* **2000**, *289*, 22.

(72) Cilwa, K. E. Surface Plasmon Polaritons and Single Dust Particles. Ph.D. Thesis, The Ohio State University, 2011.

(73) Malone, M. A. Infrared Microspectroscopy: A Study of the Single Isolated Bread Yeast Cell. M.S. Thesis, The Ohio State University, 2010.

(74) Malone, M. A.; Prakash, S.; Heer, J. M.; Corwin, L. D.; Cilwa, K. E.; Coe, J. V. *J. Chem. Phys.* **2010**, *133*, 185101.

(75) van de Hulst, H. C. *Light Scattering by Small Particles*: John Wiley and Sons: New York, 1958.

(76) Hobert, H. *Vib. Spectrosc.* **1995**, *9*, 169.

(77) Popova, S. I.; Tolstykh, T. S.; Vorobev, V. T. *Opt. Spectrosc.* **1972**, *33*, 444.

(78) Steyer, T. R.; Day, K. L.; Huffman, D. R. *Appl. Opt.* **1974**, *13*, 1586.

(79) Peterson, J. T.; Weinman, J. A. *J. Geophys. Res.* **1969**, *74*, 6947.

(80) Spitzer, W. G.; Kleinman, D. A. *Phys. Rev.* **1961**, *121*, 1324.

(81) Blatt, H.; Middleton, G. V.; Murray, R. C. *Origin of Sedimentary Rocks*, 2nd ed.; Prentice Hall: Englewood Cliffs, NJ, 1980.

(82) Long, L. L.; Querry, M. R.; Bell, R. J.; Alexander, R. W. *Infrared Phys.* **1993**, *34*, 191.

(83) Posch, T.; Baier, A.; Mutschke, H.; Henning, T. *Astrophys. J.* **2007**, *668*, 993.

(84) Lane, M. D.; Christensen, P. R. *J. Geophys. Res.* **1997**, *102*, 25581.

(85) Klein, C.; Dana, J. D.; Hurlbut, C. S.; Klein, C. *The Manual of Mineral Science*; Wiley: New York, 2002.

(86) Matsumoto, R. Y. O.; Iijima, A. *Sedimentology* **1981**, *28*, 239.

(87) Wang, D.; Wallace, A. F.; De Yoreo, J. J.; Dove, P. M. *Proc. Natl. Acad. Sci. U.S.A.* **2009**, *106*, 21511.

(88) Jung, H.-J.; Malek, M. A.; Ryu, J.; Kim, B.; Song, Y.-C.; Kim, H.; Ro, C.-U. *Anal. Chem.* **2010**, *82*, 6193.

(89) Miller, F. A.; Wilkins, C. H. *Anal. Chem.* **1952**, *24*, 1253.

(90) Hwang, H.; Ro, C.-U. *Atmos. Environ.* **2006**, *40*, 3869.

(91) Pedrotti, F. L.; Pedrotti, L. S. *Introduction to Optics*; Prentice Hall: Upper Saddle River, NJ, 1993.

(92) Rodney, W. S.; Spindler, R. J. *J. Opt. Soc. Am.* **1954**, *44*, 677.

(93) Oberdorster, G.; Sharp, Z.; Atudorei, V.; Elder, A.; Gelein, R.; Kreyling, W.; Cox, C. *Inhalation Toxicol.* **2004**, *16*, 437.